IEEE Access
Multidisciplinary | Rapid Review | Open Access Journal

Received September 30, 2018, accepted October 17, 2018, date of publication October 22, 2018,
date of current version November 19, 2018.

Digital Object Identifier 10.1109/ACCESS.2018.2877425

Dual-Band Annular Slot Antenna Loaded by Reactive Components for Dual-Sense Circular Polarization With Flexible Frequency Ratio

JIANXING LI[1], (Member, IEEE), JUNWEI SHI[1], LUMEI LI[2], TAYYAB ALI KHAN[1], JUAN CHEN[3], (Member, IEEE), YINGSONG LI[4], (Member, IEEE), AND ANXUE ZHANG[1]

[1]School of Electronic and Information Engineering, Xi'an Jiaotong University, Xi'an 710049, China
[2]Fujian Radio Monitoring Station, State Radio Monitoring Center, Xiamen 361004, China
[3]Shenzhen Research School, Xi'an Jiaotong University, Shenzhen 518057, China
[4]College of Information and Communication Engineering, Harbin Engineering University, Harbin 150001, China

Corresponding author: Anxue Zhang (anxuezhang@mail.xjtu.edu.cn)

This work was supported in part by the National Natural Science Foundation of China under Grant 61801369, in part by the Natural Science Foundation of Shaanxi Province under Grant 2018JQ6081, in part by the China Postdoctoral Science Foundation under Grant 2018M631161, in part by the Shaanxi Province Postdoctoral Science Foundation under Grant 2017BSHYDZZ14, in part by the Fundamental Research Funds for the Central Universities under Grants XJTU1191329860 and HEUCFM180806, and in part by the Technology Program of Shenzhen under Grant JCYJ20170816100722642.

ABSTRACT This paper proposes a new design of dual-band reactively loaded annular slot antenna for dual-sense circular polarization radiation. Two concentric annular slots excited by a common microstrip feedline are employed to realize dual-band operation. Each slot can radiate a circularly polarized (CP) wave with a specified sense at its one or one-and-a-half wavelength resonance, given that an appropriately valued reactive component, i.e., capacitor or inductor, is introduced at a pre-determined location. A small frequency ratio (FR) can be achieved between the two oppositely sensed CP bands when a capacitor and an inductor are loaded, respectively, onto the inner and outer annular slots. Contrarily, two oppositely sensed CP bands that possess a large FR can be yielded when an inductor and a capacitor are loaded onto the inner and outer annular slots, respectively. For experimental verification, two antenna prototypes with FRs of 1.63 and 2.41 have been designed, fabricated, and measured. The measurement results exhibit a good agreement with the simulated ones. Details of design concerns and experimental results are presented and discussed.

INDEX TERMS Annular slot antenna (ASA), circularly polarized (CP) antenna, dual-band antenna, dual-sense circular polarization, frequency ratio (FR), reactive component.

I. INTRODUCTION

Circularly polarized (CP) antennas have become more and more desirable in modern wireless communications such as mobile communication systems [1], satellite navigation and communication systems [2]–[4], wireless local area networks (WLAN) [5], and radio frequency identification (RFID) [6]. This is because that it can provide more flexible orientation between transmitter and receiver antennas, less polarization mismatch loss, higher suppression of multipath propagation effect, stronger weather penetration, and better immunity to Faraday's rotation. In comparison with patch antennas, slot antennas have advantages including easier implementation of multiband, wider potential bandwidth, and more stability to fabrication tolerances. Therefore, slot antennas have been being one of the preferred candidates to realize CP antennas in the last several decades [7]–[11]. However, these designs can only radiate single-sense CP waves at a time, i.e. right-handed CP (RHCP) or left-handed CP (LHCP) waves.

Antennas with dual-band and dual-sense CP radiation are required in scenarios where both RHCP and LHCP signals need to be tackled in two distinct bands. For example, the receivers of Chinese Compass Navigation Satellite System (CNSS) transmit LHCP signals in the uplink L-band (1616 MHz) and receive RHCP signals in the downlink S-band (2492 MHz) [3]. Additionally, other promising applications involve multichannel communications where dual-sense CP antennas can intrinsically enhance interchannel isolation. A number of researches can be found in the literature on dual-band dual-sense CP slot antenna designs. Bao and Ammann [12], [13] have employed an annular slot

TABLE 1. Structural parameters of the CL-ASA and IL-ASA.

Ant.	W_f (mm)	W_s (mm)	L_s (mm)	R_a (mm)	R_b (mm)	C_v (pF)	L_v (nH)
CL-ASA	3.0	6.0	9.0	13.8	11.8	0.5	---
IL-ASA	3.0	2.0	18.8	18.8	16.8	---	1.8

augmented by four unequal linear slots and monofilar spiral slots to construct dual-band and dual-sense CP antennas. In [14], a dual-band coplanar waveguide (CPW)-fed slot antenna loaded by two spiral slots was shown, which can radiate LHCP and RHCP waves in the lower and upper bands, respectively. Based on C-shaped grounded strips [15] and the combination of an annular slot and a cross slot [16], dual-band dual-sense CP characteristics have also been obtained. We have proposed a dual-band annular slot antenna (ASA) with dual-sense CP radiation with the use of two concentric annular slots and capacitive components [17]. However, each operation band within most of these antennas is achieved by an individual radiating element which resonates at its fundamental mode [12], [14]–[17]. The realizable frequency ratio (FR), therefore, mainly depends on the geometrical dimensions of radiating elements in charge of the lower and upper bands. Moreover, the antenna design in [13] utilizes the fundamental and first harmonic resonances of a monofilar spiral slot to generate two frequency bands. This technique, however, results in an almost constant FR.

In this paper, a new design of a dual-band dual-sense CP ASA with a flexible FR is presented and investigated. The antenna makes use of two concentric annular slots coupled to a common microstrip feedline, aimed to fulfill dual-band operation. Each slot can be adjusted to resonate at its one or one-and-a-half wavelength mode by employing a capacitor or an inductor. Hence, those two operation bands are jointly determined by geometrical dimensions and resonant modes of the annular slots, and consequently, a flexible FR with a wide tuning range can be ensured. Given a properly valued and located reactive component, a particular CP sense can be assigned to each band, and as a result, a dual-sense CP radiation can be readily achieved. The proposed concept is demonstrated by both simulations and measurements of two prototypes loaded with distributed reactive components, i.e. a distributed capacitor and a distributed inductor. The first prototype exhibits a small FR of 1.63, and radiates a RHCP wave in the lower band (1847 MHz) and a LHCP wave in the upper band (3005 MHz). The second prototype owns a large FR of 2.41, and attains LHCP and RHCP properties in the lower and upper bands, respectively, i.e. 1552 MHz and 3741 MHz. Throughout this paper, the full-wave simulator Ansoft HFSS is used to perform the simulations.

II. CP ASAS LOADED WITH REACTIVE COMPONENTS

The effectiveness of introducing a reactive component across a traditional microstrip line-fed annular slot for achieving CP radiation is firstly demonstrated in this section.

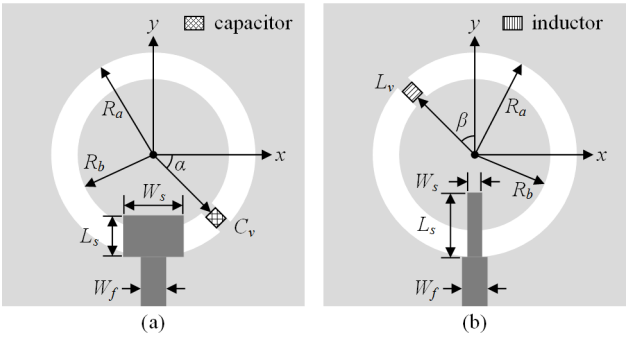

FIGURE 1. Schematic layouts of two reactively loaded CP ASAs. (a) CL-ASA. (b) IL-ASA.

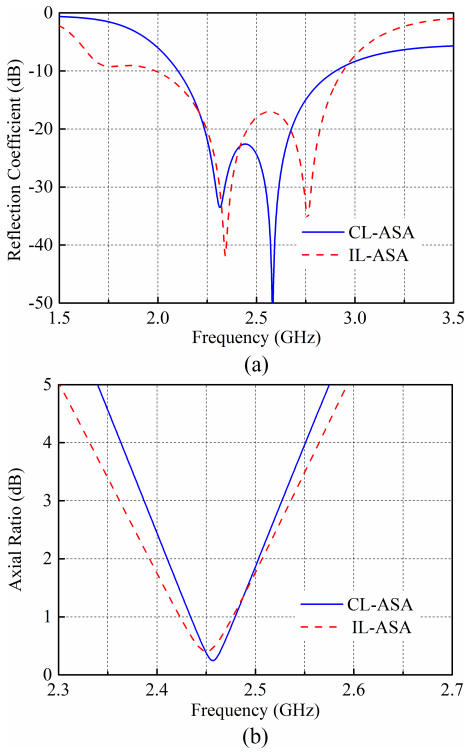

FIGURE 2. Simulated (a) reflection coefficients and (b) broadside ARs of the CL-ASA and IL-ASA.

Figs. 1(a) and (b) depict the schematic layouts of two CP ASAs loaded with a lumped capacitor and a lumped inductor, respectively. The former is indicated as CL-ASA while the latter is indicated as IL-ASA. The ground plane printed on the upper layer of the substrate is etched by an annular slot. A microstrip feedline is printed on the bottom layer of the substrate, which is stepped to enhance impedance matching. The substrate is a 50 mm × 50 mm FR-4 board with a relative permittivity of 4.4, a loss tangent of 0.02, and a thickness of 1.6 mm. Table 1 concludes the optimal structural parameters. We should remind that for any position along the annular slot, there theoretically exists an optimum valued reactive component, producing excellent CP performance. In this work, for simplicity, the positions of the capacitor

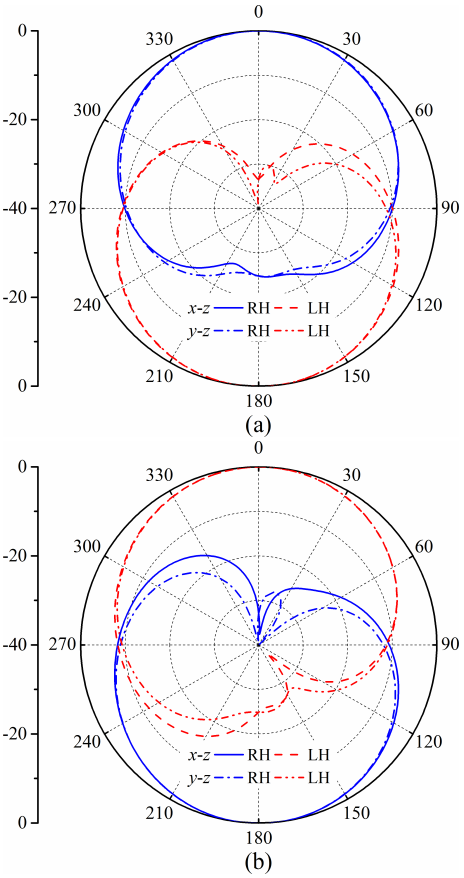

FIGURE 3. Simulated farfield radiation patterns of the (a) CL-ASA and (b) IL-ASA.

and inductor are selected as $\alpha = \beta = 45°$, which results in $C_v = 0.5$ pF and $L_v = 1.8$ nH, respectively.

The simulated reflection coefficients and broadside axial ratios (ARs) of the CL-ASA and IL-ASA are, respectively, illustrated in Fig. 2. In detail, the CL-ASA achieves a 10 dB impedance bandwidth of 799 MHz ranging from 2103 MHz to 2902 MHz and a 3 dB AR bandwidth of 139 MHz from 2387 MHz to 2526 MHz. With respect to the IL-ASA, the 10 dB impedance and 3 dB AR bandwidths are 951 MHz ranging from 1988 MHz to 2939 MHz and 173 MHz from 2362 MHz to 2535 MHz, respectively.

Fig. 3(a) shows the farfield radiation patterns of the CL-ASA in both the *x*-*z* and *y*-*z* planes, simulated at 2457 MHz where a minimum AR of 0.25 dB occurs. It clearly obtains a RHCP sense in the upper hemisphere and a LHCP sense in the lower hemisphere due to the image theory. Fig. 3(b) shows the farfield radiation patterns of the IL-ASA at 2450 MHz with a minimum AR of 0.41 dB. Contrarily to the CL-ASA, the IL-ASA exhibits LHCP and RHCP senses in the upper and lower hemispheres, respectively. We further find that the radiation patterns of both antennas slightly deviate from the broadside directions. This is because the structural symmetry is destroyed by the loaded reactive components.

TABLE 2. Relationship between the CP sense and the reactive component type and its positioned quadrant.

Ant.	Type	Quad. I	Quad. II	Quad. III	Quad. IV
CL-ASA	Capacitor	LHCP	RHCP	LHCP	RHCP
IL-ASA	Inductor	RHCP	LHCP	RHCP	LHCP

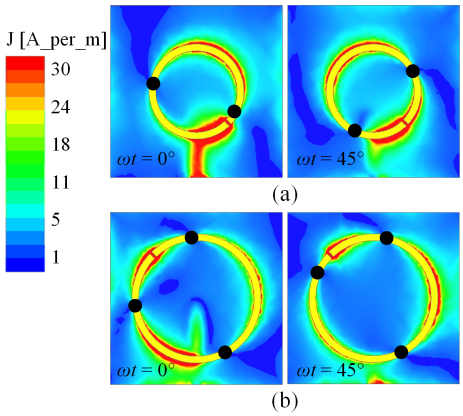

FIGURE 4. Simulated surface current distribution of the (a) CL-ASA and (b) IL-ASA. The dark dot represents the surface current null.

Close inspection reveals that the CP sense of the reactively loaded ASA depends on the reactive component type and its position with respect to the microstrip feedline. As to the CL-ASA and IL-ASA illustrated in Fig. 1, Table 2 details and summarizes the relationship between the CP sense and the positioned quadrant of the reactive component loaded in the *x*-*y* plane.

Observing the surface current distribution can identify the resonant mode of the reactively loaded ASA. Fig. 4 presents the simulated surface current distribution of the CL-ASA and IL-ASA, respectively, at different time instants. The dark dot represents the surface current null. Obviously, there exist two current nulls along the annular slot in the CL-ASA, implying that it is operated at its one wavelength resonance. Different from the CL-ASA, three current nulls can be observed along the annular slot in the IL-ASA, suggesting that it works at its one-and-a-half wavelength resonance. As a consequence, the operation band of the CP ASA can be determined jointly by the geometrical dimension and resonant mode of the annular slot. Moreover, we can notice that the surface current of the CL-ASA is revolved in a counter-clockwise direction with time, whereas that of the IL-ASA travels in a clockwise direction with time, further confirming the obtained RHCP and LHCP senses in the upper hemisphere.

III. DUAL-BAND DUAL-SENSE CP ASAS OF FLEXIBLE FRs

In accordance to the above investigation, it is straightforward to understand that, with the employment of a properly valued reactive component at an appropriate position, the microstrip line-fed ASA can realize any specific CP sense with flexibly manipulated resonant frequencies. This fact is very beneficial

TABLE 3. Structural parameters of the ANT1 and ANT2.

Ant.	R_o (mm)	R_i (mm)	W_r (mm)	G_d (mm)	W_d (mm)	L_f (mm)	W_f (mm)	L_m (mm)	W_m (mm)	L_t (mm)	W_t (mm)	α (°)	β (°)	φ_o (°)	φ_i (°)
Ant1	20.8	12.2	2.0	0.1	0.6	8.0	3.0	8.7	2.2	15	3.0	40	80	-135	45
Ant2	21.2	12.3	2.0	0.1	0.6	5.0	3.0	8.3	0.5	18.0	0.5	42	30	-135	-135

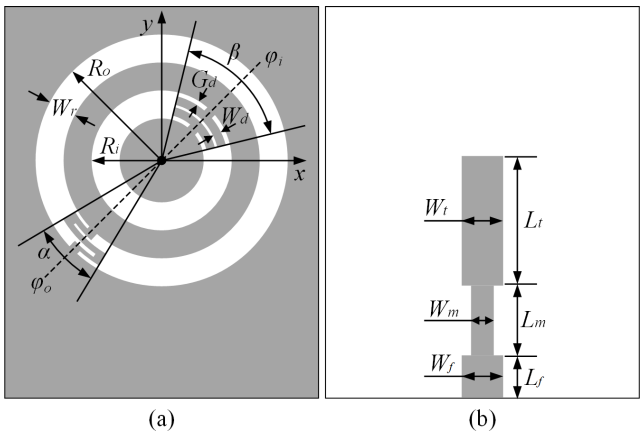

FIGURE 5. Geometrical layout of the proposed Ant1.

to develop a dual-band oppositely-sensed CP ASA in a wide FR range.

To demonstrate the design concept, two antenna examples are proposed and implemented, both of which are constructed on a 1.6 mm thick and 65 mm × 55 mm size FR-4 substrate with a relative permittivity of 4.4 and a loss tangent of 0.02. Each antenna comprises two concentric annular slots coupled to a common stepped microstrip feedline. The Ant1 featuring a small FR exhibits a RHCP sense in the lower band and a LHCP sense in the upper band. Dissimilarly, the Ant2 has a large FR, and radiates LHCP and RHCP waves, respectively, in the lower and upper bands. It should be noted that the CP sense in the upper hemisphere is defined as that of the ASA.

In the simulations, the reactive components are resembled initially using ideal lumped *RLC* boundaries and afterwards substituted by corresponding distributed ones. In specific, the necessary capacitance is provided by two tightly spaced and coupled arc-shaped strips while a meandered grounded strip is employed to offer the required inductance.

A. ANALYSIS AND RESULTS OF THE ANT1

Fig. 5 presents the geometrical layout of the Ant1, wherein a distributed capacitor and a distributed inductor are introduced across the inner and outer annular slots, respectively. Hence, the inner annular slot can excite a LHCP radiation at its one wavelength resonance and the outer annular slot can ensure a RHCP one at its one-and-a-half wavelength resonance. As a result, a small FR between the upper and lower bands can be yielded. The final structural parameters of the Ant1 are given in Table 3.

The simulated and measured reflection coefficients as well as broadside ARs of the Ant1 are contrasted in Fig. 6. Fairly

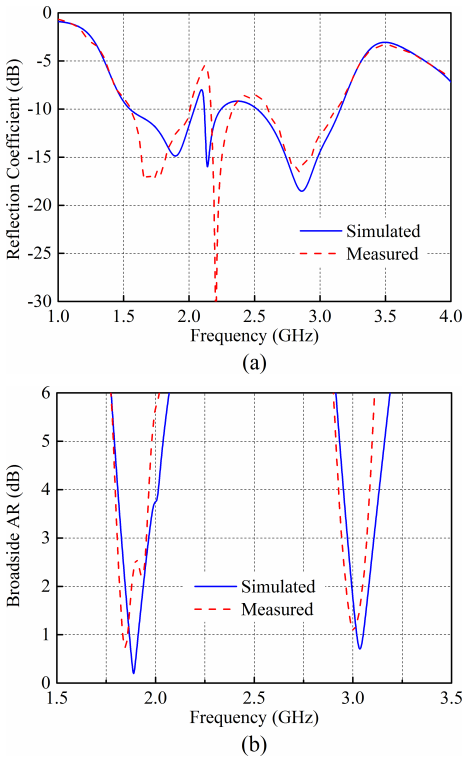

FIGURE 6. Reflection coefficients and broadside ARs of the Ant1. (a) Reflection coefficients. (b) Broadside ARs.

good correspondence can be observed between the measured and simulated results. Errors are most probably owing to the fabrication imperfections. The measurements show the 10 dB impedance and 3 dB AR bandwidths to be 455 MHz (1553 MHz to 2008 MHz) and 149 MHz (1805 MHz to 1954 MHz) or about 24.6% and 8.1% relative to the center frequency of 1847 MHz for the lower band. Here, we should note that the center frequency denotes the frequency where minimum AR appears. For the upper band, the measured 10 dB impedance and 3 dB AR bandwidths are 528 MHz (2603 MHz to 3131 MHz) and 129 MHz (2942 MHz to 3071 MHz) or 17.6% and 4.3% approximately relative to the center frequency of 3005 MHz. Thus, a FR of 1.63 between the upper and lower bands is obtained.

The simulated and measured radiation patterns in both the *x*-*z* and *y*-*z* planes, respectively, at 1889 MHz and 3036 MHz are normalized and shown in Fig. 7. Reasonable agreement is maintained between the measured and simulated results. The RHCP radiation pattern at 1889 MHz is squinted by 7° in the *x*-*z* plane with a 3 dB beamwidth of 95° and deviated by 4° in the *y*-*z* plane with a 3 dB beamwidth of 84°. At 3036 MHz,

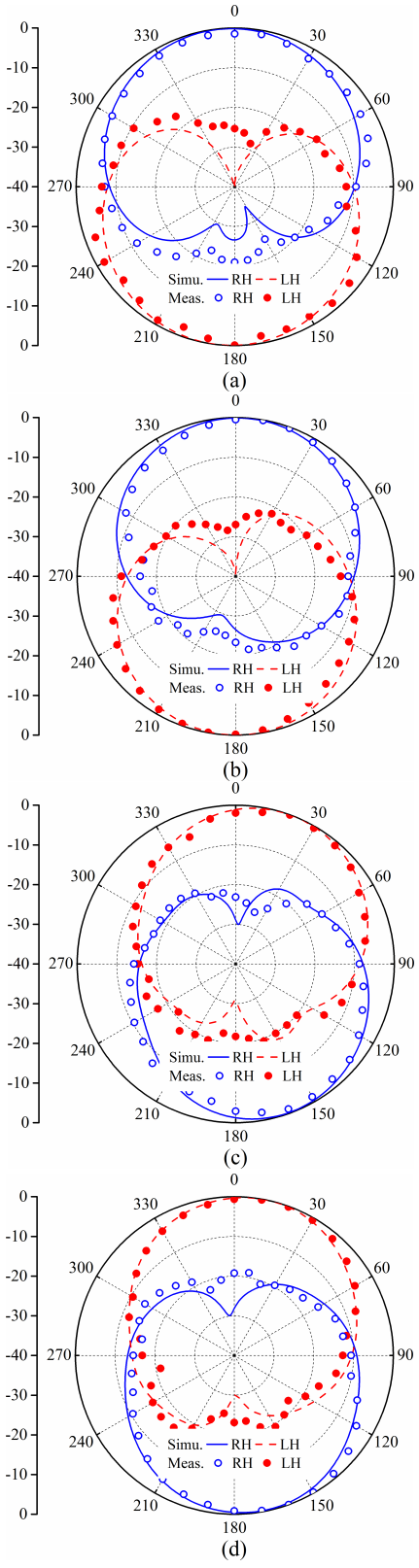

FIGURE 7. Radiation patterns of the Ant1. (a) *x-z* plane and (b) *y-z* plane at 1889 MHz. (c) *x-z* plane and (d) *y-z* plane at 3036 MHz.

it shows the LHCP radiation pattern to be offset by 21° in the *x-z* plane with a beamwidth of 80° and diverged by 11° in the *y-z* plane with a beamwidth of 70°.

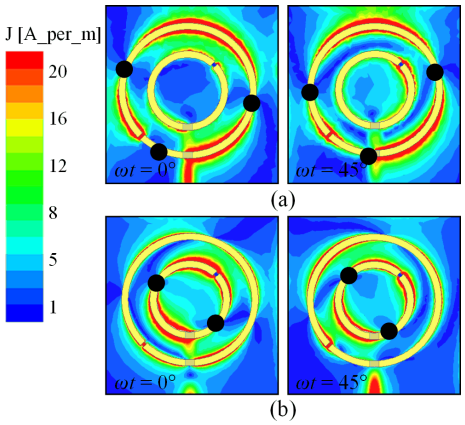

FIGURE 8. Surface current distribution of the Ant1. (a) 1889 MHz. (b) 3036 MHz. The dark dot represents the surface current null.

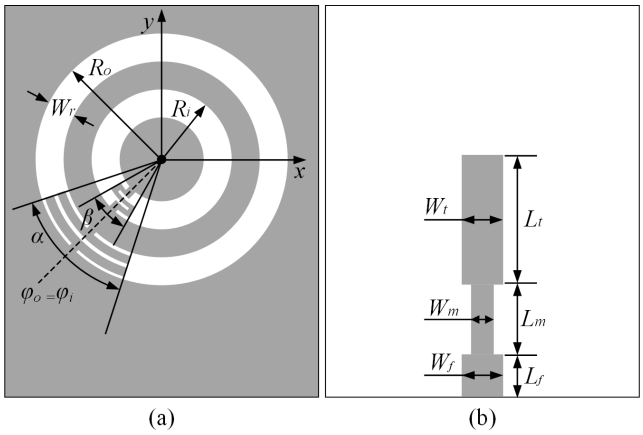

FIGURE 9. Geometrical layout of the proposed Ant2. Parameters of W_d and G_d are not indicated for conciseness.

Within the 3 dB AR bandwidths, the measured realized CP gains are from 2.5 dBic to 3.2 dBic in the lower band and 3.7 dBic to 4.9 dBic in the upper band. Moreover, the simulated radiation efficiency is larger than 80% in the lower CP band and around 90% in the upper CP band.

Fig. 8 illustrates the simulated surface current distribution with time. The surface current has three distribution nulls and a counter-clockwise rotation at 1889 MHz, implying a one-and-a-half wavelength resonance and RHCP radiation. As for 3036 MHz, two current nulls and a clockwise circulation can be recognized, which guarantees a one wavelength resonance and LHCP radiation.

B. ANALYSIS AND RESULTS OF THE ANT2

The geometrical layout of the Ant2 is depicted in Fig. 9 that utilizes a distributed inductor along the inner annular slot and a distributed capacitor along the outer annular slot. A RHCP sense can therefore be obtained for the inner annular slot at its one-and-a-half wavelength resonance and a LHCP sense can be acquired at its one wavelength resonance for the outer annular slot. Resultantly, the upper and lower bands can have a larger FR. Details of optimal structural parameters of the Ant2 can be found in Table 3.

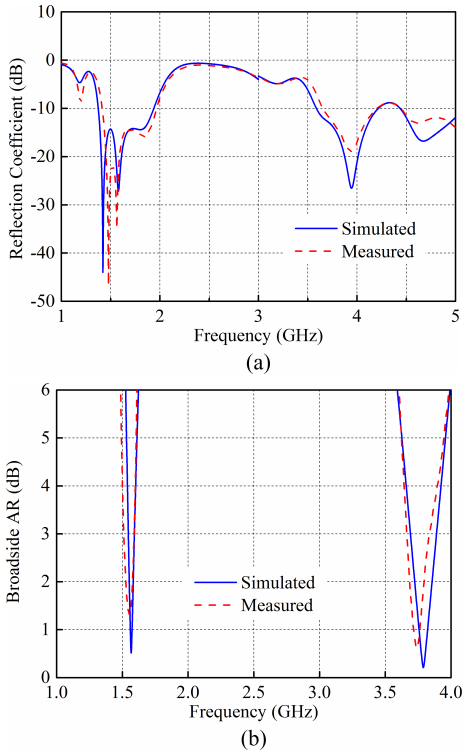

FIGURE 10. Reflection coefficients and broadside ARs of the Ant2. (a) Reflection coefficients. (b) Broadside AR.

Fig. 10 compares the measured reflection coefficients and boresight ARs with the simulated ones of the Ant2, which are also in good consistency. The measured results show that the 10 dB impedance bandwidth is 551 MHz (1413 MHz to 1964 MHz) and the 3 dB AR bandwidth is 77 MHz (1510 MHz to 1587 MHz), i.e. about 35.5% and 4.9% with regard to the center frequency of 1552 MHz in the first operation band. As in the second operation band, the measured 10 dB impedance bandwidth is exhibited to be 546 MHz (3652 MHz to 4198 MHz) and the 3 dB AR bandwidth is shown to be 171 MHz (3663 MHz to 3834 MHz), i.e. almost 14.6% and 4.6% with regard to the center frequency of 3741 MHz. Consequently, the FR between the second and first operation bands is 2.41.

Fig. 11 depicts the normalized radiation patterns simulated and measured at 1568 MHz and 3788 MHz, respectively, in both the *x*-*z* and *y*-*z* planes. Unlike to the Ant1, the Ant2 has a LHCP sense in the first operation band and a RHCP sense in the second operation band. A symmetrical LHCP radiation pattern can be found with 3 dB beamwidths of 99° and 86° in the *x*-*z* and *y*-*z* planes, respectively, at 1568 MHz. The RHCP radiation pattern at 3788 MHz is diverged by 8° with a 3 dB beamwidth of 74° in the *x*-*z* plane and deflected by 10° with a 3 dB beamwidth of 86° in the *y*-*z* plane.

The measured realized peak CP gain is fluctuated between 2.9 dBic and 3.4 dBic and between 4.2 dBic and 4.7 dBic in the first and second operation bands, respectively, across the 3 dB AR bandwidths. Furthermore, the simulated radiation efficiencies are above 85% in both operation bands.

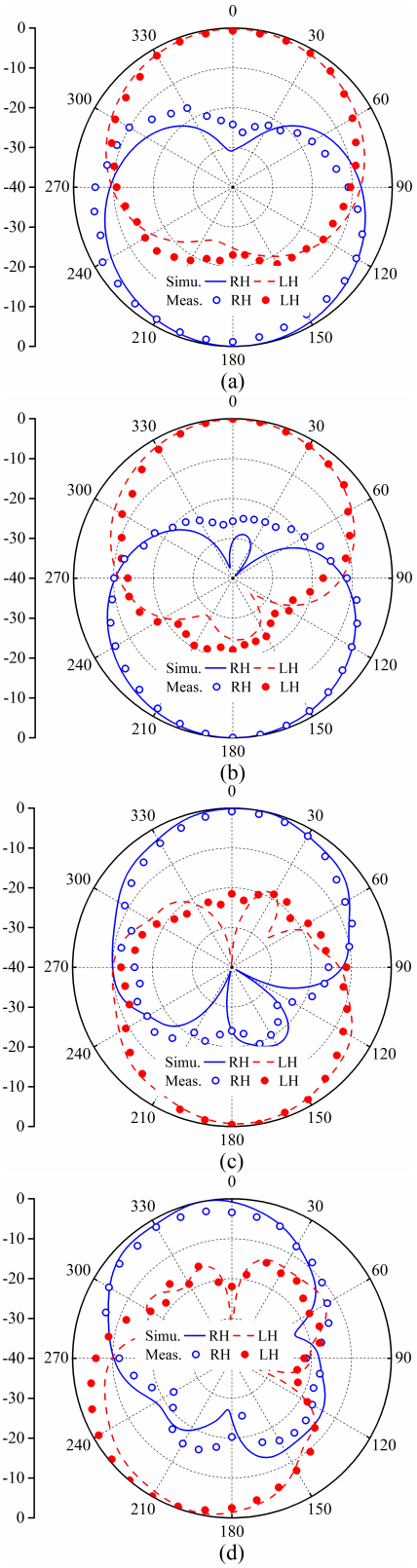

FIGURE 11. Radiation patterns of the Ant2. (a) *x*-*z* plane and (b) *y*-*z* plane at 1568 MHz. (c) *x*-*z* plane and (d) *y*-*z* plane at 3788 MHz.

The simulated surface current distribution at different time instants are illustrated in Fig. 12. At 1568 MHz, two surface current nulls are identified traveling in a clockwise

TABLE 4. Performance comparison between the Ant1 and Ant2.

Ant.	FR	Lower Band				Upper Band			
		f_L (MHz)	CP Sense	IMBW (MHz, %)	ARBW (MHz, %)	f_H (MHz)	CP Sense	IMBW (MHz, %)	ARBW (MHz, %)
Ant1	1.63	1847	RHCP	455, 24.6	149, 8.1	3005	LHCP	528, 17.6	129, 4.3
Ant2	2.41	1552	LHCP	551, 35.5	77, 4.9	3741	RHCP	546, 14.6	171, 4.6

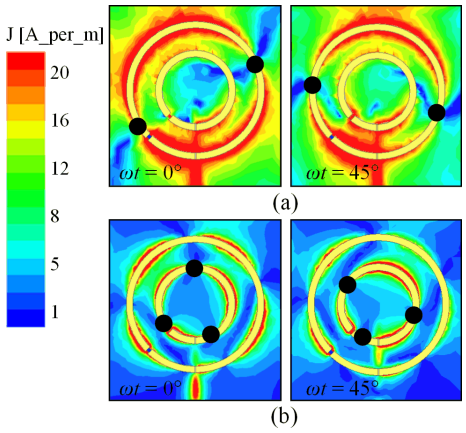

FIGURE 12. Surface current distribution of the Ant2. (a) 1568 MHz. (b) 3788 MHz. The dark dot represents the surface current null.

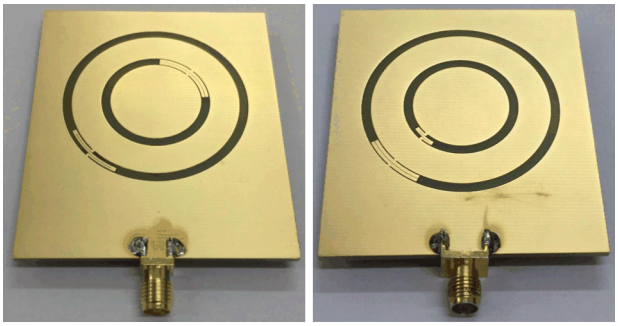

FIGURE 13. Photographs of the two fabricated antenna prototypes. (a) Ant1. (b) Ant2.

direction which demonstrates a one wavelength resonance and LHCP radiation are obtained. The current distribution exhibits three nulls and circulates in a counter-clockwise direction at 3788 MHz, suggesting that a one-and-a-half wavelength resonance and RHCP radiation are achieved.

Fig. 13 presents the photographs of the antenna prototypes. Table 4 concludes the performance comparison between the Ant1 and Ant2 in terms of circular polarization senses, center frequencies, FRs, as well as impedance and AR bandwidths. In Table 4, the f_L and f_H are the center frequencies of the lower and upper bands, respectively; the IMBW and ARBW are the impedance and AR bandwidths, respectively.

IV. CONCLUSION

This paper has investigated a novel design concept of loading conventional ASAs with reactive components to realize dual-band dual-sense CP operation. The versatility and flexibility of the proposed technique in controlling the CP sense and FR have been demonstrated thoroughly. Two oppositely-sensed antenna prototypes with a FR of 1.63 and 2.41, respectively, have been fabricated and measured. The measurements well agree with simulations, and both exhibit that good impedance matching and CP radiation have been achieved within each frequency band. Besides, the proposed technique allows the realization of dual-band dual-sense CP ASAs with an even smaller or larger FR. Therefore, owing to its simple structure and flexible CP sense and FR reconfigurability, the proposed antennas can be used in wireless communications requiring dual-band dual CP reception and also can find applications in multichannel and multipolarized communications to enhance interchannel isolation.

REFERENCES

[1] W. Lin, R. W. Ziolkowski, and T. C. Baum, "28 GHz compact omnidirectional circularly polarized antenna for device-to-device communications in the future 5G systems," *IEEE Trans. Antennas Propag.*, vol. 65, no. 12, pp. 6904–6914, Dec. 2017.

[2] Nasimuddin, X. Qing, and Z. N. Chen, "A compact circularly polarized slotted patch antenna for GNSS applications," *IEEE Trans. Antennas Propag.*, vol. 62, no. 12, pp. 6506–6509, Dec. 2014.

[3] J. Li, H. Shi, H. Li, and A. Zhang, "Quad-band probe-fed stacked annular patch antenna for GNSS applications," *IEEE Antennas Wireless Propag. Lett.*, vol. 13, pp. 372–375, 2014.

[4] M. Ferrando-Rocher, J. I. Herranz-Herruzo, A. Valero-Nogueira, and A. Vila-Jiménez, "Single-layer circularly-polarized *Ka*-band antenna using gap waveguide technology," *IEEE Trans. Antennas Propag.*, vol. 66, no. 8, pp. 3837–3845, Aug. 2018.

[5] S. X. Ta, I. Park, and R. W. Ziolkowski, "Circularly polarized crossed dipole on an HIS for 2.4/5.2/5.8-GHz WLAN applications," *IEEE Antennas Wireless Propag. Lett.*, vol. 12, pp. 1464–1467, 2013.

[6] C. Raviteja, C. Varadhan, M. Kanagasabai, A. K. Sarma, and S. Velan, "A fractal-based circularly polarized UHF RFID reader antenna," *IEEE Antennas Wireless Propag. Lett.*, vol. 13, pp. 499–502, 2014.

[7] K.-L. Wong, C.-C. Huang, and W.-S. Chen, "Printed ring slot antenna for circular polarization," *IEEE Trans. Antennas Propag.*, vol. 50, no. 1, pp. 75–77, Jan. 2002.

[8] S. L. S. Yang, A. A. Kishk, and K. F. Lee, "Wideband circularly polarized antenna with L-shaped slot," *IEEE Trans. Antennas Propag.*, vol. 56, no. 6, pp. 1780–1783, Jun. 2008.

[9] C.-S. Lin, L.-T. Chen, T.-R. Chen, and J.-S. Row, "Dual-band ring slot antenna with circular polarization," *Microw. Opt. Technol. Lett.*, vol. 55, no. 9, pp. 2077–2080, 2013.

[10] C.-Y.-D. Sim, Y.-J. Liao, and H.-L. Lin, "Polarization reconfigurable eccentric annular ring slot antenna design," *IEEE Trans. Antennas Propag.*, vol. 63, no. 9, pp. 4152–4155, Sep. 2015.

[11] J. Li, C. Wang, A. Zhang, W. Joines, and Q. Liu, "Microstrip-line-fed reactively loaded circularly polarized annular-ring slot antenna," *J. Electromagn. Waves Appl.*, vol. 31, no. 1, pp. 101–110, 2017.

[12] X. Bao and M. J. Ammann, "Dual-frequency dual-sense circularly-polarized slot antenna fed by microstrip line," *IEEE Trans. Antennas Propag.*, vol. 56, no. 3, pp. 645–649, Mar. 2008.

[13] X. L. Bao and M. J. Ammann, "Monofilar spiral slot antenna for dual-frequency dual-sense circular polarization," *IEEE Trans. Antennas Propag.*, vol. 59, no. 8, pp. 3061–3065, Aug. 2011.
[14] C. Chen and E. K. N. Yung, "Dual-band dual-sense circularly-polarized CPW-fed slot antenna with two spiral slots loaded," *IEEE Trans. Antennas Propag.*, vol. 57, no. 6, pp. 1829–1833, Jun. 2009.
[15] Y.-Y. Chen, Y.-C. Jiao, G. Zhao, F. Zhang, Z.-L. Liao, and Y. Tian, "Dual-band dual-sense circularly polarized slot antenna with a C-shaped grounded strip," *IEEE Antennas Wireless Propag. Lett.*, vol. 10, pp. 915–918, 2011.
[16] Y. Shao and Z. Chen, "A design of dual-frequency dual-sense circularly-polarized slot antenna," *IEEE Trans. Antennas Propag.*, vol. 60, no. 11, pp. 4992–4997, Nov. 2012.
[17] C. Wang, J. Li, A. Zhang, W. T. Joines, and Q. H. Liu, "Dual-band capacitively loaded annular-ring slot antenna for dual-sense circular polarization," *J. Electromagn. Waves Appl.*, vol. 31, no. 9, pp. 867–878, 2017.

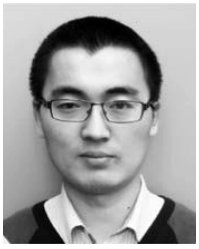

JIANXING LI (S'15–M'18) received the B.S., M.S., and Ph.D. degrees in electromagnetic field and microwave technology from Xi'an Jiaotong University, Xi'an, China, in 2008, 2011, and 2016, respectively. From 2014 to 2016, he was a Visiting Researcher with the Department of Electrical and Computer Engineering, Duke University, Durham, NC, USA, under the financial support from the China Scholarship Council.

He is currently a Lecturer with the School of Electronic and Information Engineering, Xi'an Jiaotong University. His current research interests include antennas, microwave and millimeter-wave circuits, and metamaterials. He serves as a reviewer for several international journals including the IEEE Access, the *IET Electronics Letters*, the *International Journal of RF and Microwave Computer-Aided Engineering*, and the *International Journal of Electronics and Communications*.

JUNWEI SHI received the B.S. degree in information engineering from Xi'an Jiaotong University, Xi'an, China, in 2018, where she is currently pursuing the M.S. degree in electronic and communication engineering with the Electromagnetics and Communication Laboratory. Her current research interests include reconfigurable antennas and metamaterials.

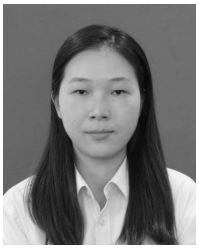

LUMEI LI received the B.S. degree in microelectronics and the M.S. degree in electromagnetic field and microwave technology from Xi'an Jiaotong University, Xi'an, China, in 2014 and 2017, respectively. From 2012 to 2014, she was a government-funded Student in electronic science and technology with the Ecole Centrale de Marseille, France.

She is currently an Assistant Engineer with the Fujian Radio Monitoring Station, State Radio Monitoring Center, Xiamen, China. Her current research interests include antennas and radio monitoring.

TAYYAB ALI KHAN received the B.S. degree in electrical engineering from the University of Central Punjab, Lahore, Pakistan, in 2017. He is currently pursuing the M.S. degree in information and communication engineering with the Electromagnetics and Communication Laboratory, Xi'an Jiaotong University, Xi'an, China. His current research interests include antennas and metamaterials.

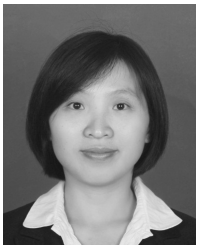

JUAN CHEN (M'18) received the Ph.D. degree in electromagnetic field and microwave technology from Xi'an Jiaotong University, Xi'an, China, in 2008. From 2016 to 2017, she was a Visiting Researcher with the Department of Electrical and Computer Engineering, Duke University, Durham, NC, USA, under the financial support from the China Scholarship Council.

She is currently a Professor with the Shenzhen Research School and also with the School of Electronic and Information Engineering, Xi'an Jiaotong University, Xi'an, China. Her current research interests include numerical electromagnetic methods, advanced antenna designs, and graphene theory and application.

YINGSONG LI (M'14) received the B.S. degree in electrical and information engineering and the M.S. degree in electromagnetic field and microwave technology from Harbin Engineering University, Harbin, China, in 2006 and 2011, respectively, and the Ph.D. degree from the Kochi University of Technology (KUT), Japan, and Harbin Engineering University in 2014.

He was a Visiting Scholar with the University of California, Davis, from 2016 to 2017, and also with the University of York, U.K., in 2018. He has been a Full Professor with Harbin Engineering University since 2014. He is currently a Visiting Professor with Far Eastern Federal University and KUT. He is a Senior Member of the Chinese Institute of Electronics. He is an Associate Editor of the IEEE Access and the *Applied Computational Electromagnetics Society Journal*, and he is also an Area Editor of the *AEÜ-International Journal of Electronics and Communications*.

His current research interests include remote sensing, underwater communications, signal processing, radar, SAR imaging, compressed sensing, and antennas. He serves as a reviewer for more than 20 journals.

ANXUE ZHANG received the B.S. degree in electrical and electronics engineering from Henan Normal University, Xinxiang, China, in 1996, and the M.S. and Ph.D. degrees in electromagnetic fields and microwave technology from Xi'an Jiaotong University, Xi'an, China, in 1999 and 2003, respectively.

He is currently a Professor with the School of Electronic and Information Engineering, Xi'an Jiaotong University. His current research interests include antennas and electromagnetic wave propagation, RF and microwave circuit design, array signal processing, and metamaterials.